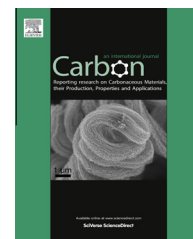


Available at [www.sciencedirect.com](http://www.sciencedirect.com)

SciVerse ScienceDirect

journal homepage: [www.elsevier.com/locate/carbon](http://www.elsevier.com/locate/carbon)

# Synthesis and supercapacitor performance studies of N-doped graphene materials using o-phenylenediamine as the double-N precursor

Yanhong Lu <sup>a,b,c</sup>, Fan Zhang <sup>b</sup>, Tengfei Zhang <sup>b</sup>, Kai Leng <sup>b</sup>, Long Zhang <sup>b</sup>, Xi Yang <sup>b</sup>, Yanfeng Ma <sup>b</sup>, Yi Huang <sup>b</sup>, Mingjie Zhang <sup>a,\*</sup>, Yongsheng Chen <sup>b,\*</sup>

<sup>a</sup> Department of Chemistry, School of Sciences, Tianjin University, Weijin Road 92, Tianjin 300072, China

<sup>b</sup> Key Laboratory of Functional Polymer Materials and Center for Nanoscale Science and Technology, Institute of Polymer Chemistry, College of Chemistry, Nankai University, Weijin Road 94, Tianjin 300071, China

<sup>c</sup> School of Chemistry & Material Science, Langfang Teachers College, Langfang, Hebei 065000, China

## ARTICLE INFO

### Article history:

Received 5 March 2013

Accepted 7 July 2013

Available online 13 July 2013

## ABSTRACT

N-doped graphene (NG) materials have been prepared through a one-step solvothermal reaction by using o-phenylenediamine as a double-N precursor. N-doping and reduction of graphene oxide (GO) are both achieved simultaneously during the solvothermal reaction. The results of scanning electron microscopy and high resolution transmission electron microscopy measurements indicate that NG is highly crumpled. And the N-doping is confirmed by elemental analysis, X-ray photoelectron spectroscopy, Raman spectroscopy, Fourier transformed infrared spectroscopy and ultraviolet–visible spectroscopy. The doping level of nitrogen reaches up to 7.7 atom% and the types in NG are benzimidazole-N and phenazine-N. The NG materials exhibit excellent electrochemical performance for symmetric supercapacitors with a high specific capacitance of 301 F g<sup>-1</sup> at a current density of 0.1 A g<sup>-1</sup> in 6 M KOH electrolyte, which is remarkably higher than the solvothermal products of pristine GO (210 F g<sup>-1</sup> at 0.1 A g<sup>-1</sup>). The NG materials also exhibit superior cycling stability (97.1% retention) and coulombic efficiency (99.2%) after 4000 cycles, due to the high content of nitrogen atoms, unique types of nitrogen and improved electronic conductivity.

© 2013 Elsevier Ltd. All rights reserved.

## 1. Introduction

Electrochemical capacitors (ECs), also named supercapacitors or ultracapacitors, have attracted considerable attention in recent years attributed to their high power density, reversibility, high rate capability and long cycle life, as well as low maintenance requirements [1–3]. According to their charge storage mechanisms, ECs can be divided into electrochemical double-layer capacitors (EDLCs) and pseudo-capacitors. EDLCs store and release energy depended on the electrostatic interactions between ions in the electrolyte and the active

electrode materials, and pseudo-capacitors store energy by fast surface Faradaic redox reactions [4]. Pseudo-capacitors can obtain much higher pseudo-capacitance than EDLCs. However, the degradation of capacitance and short cycle lives of most pseudo-capacitors have limited their practical applications in industry because the redox reactions are not entirely reversible and the structure of the materials would easily damage during the redox process [5]. Compared with pseudo-capacitors, EDLCs have superior cycling stability, higher reversibility and lower cost. Nevertheless, the relatively low capacitance of EDLCs mainly in the range of 100–

\* Corresponding authors: Tel: +86 1331 207 6671 (M. Zhang) Fax: +86 2223 499992 (Y. Chen).

E-mail addresses: [mjzhangtju@163.com](mailto:mjzhangtju@163.com) (M. Zhang), [yschen99@nankai.edu.cn](mailto:yschen99@nankai.edu.cn) (Y. Chen).

0008-6223/\$ - see front matter © 2013 Elsevier Ltd. All rights reserved.

<http://dx.doi.org/10.1016/j.carbon.2013.07.026>

300 F g<sup>-1</sup> for aqueous and 90–140 F g<sup>-1</sup> for organic electrolytes [6–10] is still not satisfied with the demand of many applications. Thus, it is of great importance for building ECs with higher capacitance without sacrificing excellent cycling stability.

As a rising star in materials science and technology, graphene, with high electronic conductivity and large specific surface area (SSA), has been widely explored as electrode materials in the fields of ECs [11–14]. However, during the preparing process of graphene, the raw material graphene oxide (GO) sheets would easily get agglomerated, which would lead to the decrease of the SSA, thus exhibit much lower capacitance than the intrinsic capacitance of graphene. In order to improve the capacitance of graphene-based ECs, many methods have been reported, including the introduction of fillers or dopants to graphene, such as transition metal oxides [15–18], conducting polymers [19,20] carbon nanotubes [21–23] and heteroatoms [24], which would prevent the restacking of graphene sheets as well as increase the entire capacitance due to the additional redox-active functional groups.

Among various heteroatoms doping, N-doped graphene (NG) has attracted much attention because nitrogen atom is in a comparable size and contains five valence electrons available to form strong valence bonds with carbon atom [25]. So plenty of functional nitrogen containing groups such as pyridine and pyrrole, have been introduced into graphene [26–28]. Because the redox reactions of pyridine and pyrrole are reversible, NG utilized as electrode materials not only shows comparable capacitance to those of pseudo-capacitors but also has the robust charging mechanisms of EDLCs which would enhance the cycling stability [29].

Up to now, several methods have been employed to synthesize NG. Chemical vapor deposition in the presence of nitrogen containing precursors [30], arc discharge of graphite electrodes in a H<sub>2</sub>/pyridine or H<sub>2</sub>/NH<sub>3</sub> atmosphere [31], nitrogen plasma process [32], electrothermal reaction [33], and thermal annealing of GO with urea [34], melamine [35], and cyanamide [36] are reliable and straightforward methods to fabricate NG. However, these processes suffer from rigorous conditions and sophisticated equipments, and sometimes together with low product yield and high cost. Recently, it has been found that hydrothermal or solvothermal reaction has the merits of mild conditions, scale-up synthesis and a high N-doped level. Through this approach, urea [37], pyrrole [38], organic amine [39], hexamethylenetetramine [40] have been studied for use as the nitrogen source for NG. Above all the reported methods, with the single-N precursors as the dopants, would generate four forms of nitrogen in NG, which are pyridinic-N, pyrrolic-N, quaternary-N and pyridine-N-oxide.

In this study, NG hydrogel has been prepared through an effective one-step solvothermal reaction by using *o*-phenylenediamine (OPD) as a double-N precursor. To the best of our knowledge, there have been no reports about doping graphene using OPD as a double-N source, meanwhile with the solvothermal reaction. During the preparation process, not only the benzimidazole-N (pyrrolic-N) was formed, a new form of doping nitrogen, phenazine-N in the graphene lattice was also produced because of the double –NH<sub>2</sub> in OPD reactant (Fig. 1). Thus we can call the form as double-N, which means that there are two nitrogen atoms in each

precursor molecule and the doping process was achieved in the form of doping two nitrogen atoms in one benzene ring of graphene. The advantages of double-N doped graphene are obvious as follows. Firstly, high nitrogen level in NG can be achieved. Secondly, in the electrochemical process, the benzimidazole-N could offer high capacitance through the Faradaic redox reactions [41], and at the same time, the charging mechanisms of EDLCs and the excellent cycling stability were reserved. More importantly, the formation of the phenazine structure makes double nitrogen atoms exist in the same hexagon skeleton of benzene ring at the edge of graphene, which can not only enhance the cycling stability of supercapacitors, but also improve the electronic conductivity of the materials because of the  $\pi$ - $\pi$  conjugated system between graphene and the electron-rich nitrogen. Therefore, the supercapacitors based on our NG materials possess the dual advantages of pseudo-capacitors and EDLCs. With its stable structure, high nitrogen content and outstanding electronic conductivity, supercapacitors based on NG materials exhibit excellent electrochemical performance including high specific capacitance, good rate performance and long cycling life, implying the great potential of this material for high-performance energy storage devices.

## 2. Experimental

### 2.1. Materials synthesis

GO was synthesized by oxidation of natural graphite powder (average particle size of 20  $\mu$ m, Qingdao Huarun Graphite Co., Ltd.) using a modified Hummers method as we described elsewhere [42]. NG with high nitrogen content was synthesized through a one-step solvothermal process using OPD (Heowns Biochem Technologies LLC) as the chemical dopant in the presence of GO aqueous dispersion. Typically, GO (160 mg) and OPD (400 mg) were dispersed in deionized water (40 ml) and ethanol (40 ml) by ultrasonication, respectively. Then, the OPD solution was added into the GO solution and the mixture was ultrasonicated for 30 min. The solution was then sealed in a 100 ml Teflon-lined autoclave and heated up to 180 °C and maintained at this temperature for 12 h. The autoclave was then naturally cooled to room temperature. A hydrogel column was obtained from this process. The hydrogel was dispersed in ethanol with magnetic stirring, then filtrated and thoroughly washed several times with ethanol and acetone. Finally, the collected sample was dried in a vacuum oven at 120 °C for 12 h. For comparison, reduced GO (RG) was also prepared under the same experimental parameters but without adding the OPD into the GO aqueous dispersion. The adsorption product of RG and OPD (RG/OPD) was prepared through immersing the RG hydrogel into the OPD solution (100 mg OPD was add to 10 ml ethanol and 10 ml water mixture) for 48 h and then was dried by the above method.

### 2.2. Characterization

The structure and morphology of the products were investigated by a field emission scanning electron microscopy (FE-

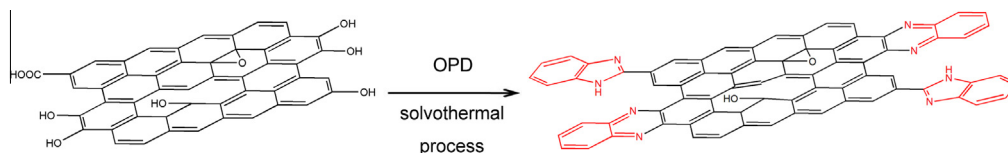


**Fig. 1** – Scheme of the possible formation mechanism of the solvothermal reaction of GO and OPD.

SEM, LEO 1530 VP) with an acceleration voltage of 10 kV, high resolution transmission electron microscopy (HR-TEM, JEOL TEM-2100) with an acceleration voltage of 200 kV and atomic force microscopy (AFM, Nanoscope IIIa Multimode 8, Bruker, operating in ScanAsyst mode) measurements. Raman scattering was performed on a Renishaw inVia Raman spectrometer using laser excitation at 514.5 nm. Fourier transform infrared (FT-IR) spectra were recorded on a Bruker Tensor 27 spectrometer (Germany). Ultraviolet and visible (UV-vis) spectra were measured with a JASCO V-570 spectrometer. X-ray photoelectron spectroscopy (XPS) analysis was obtained using AXIS HIS 165 spectrometer (Kratos Analytical) with a monochromatized Al K $\alpha$  X-ray source (1486.71 eV photons) to analyze the chemical composition of the materials. Elemental analysis was carried out at Vario Micro cube, (Elementar, Germany) for determination of the C, H, N and O content. Thermogravimetric analysis (TGA) was done by a Thermogravimetric analyzer (Mettler Toledo, TGA/DSC1) at a heating rate of 10 °C min<sup>-1</sup> under argon flow.

### 2.3. Fabrication of supercapacitors

The supercapacitor test cells were fabricated by a symmetrical two-electrode system with NG and RG materials following the recommended industry standard methods [43,44]. The electrode materials were prepared by mixing NG or RG, carbon black (Super P, Timcal) and polytetrafluoroethylene (PTFE, solid powder, Dupont) at the weight ratio of 85:5:10. The mixture was homogenized in an agate mortar, then was rolled into 80–100  $\mu$ m thickness sheets and punched into 13 mm diameter. A single typical electrode had a weight between 5.0 and 7.0 mg after dried at 120 °C for 6 h under vacuum. Then two identical (by weight) electrodes were pressed on a Ni foam ( $\varnothing$  = 13 mm) current collector and separated by a cellulose film as separator and were sandwiched in a stainless steel plate using 6 M KOH aqueous electrolyte.

### 2.4. Electrochemical measurements

The electrochemical performance and capacitance measurements of above supercapacitors were studied by cyclic voltammetry (CV), galvanostatic charge/discharge and electrochemical impedance spectroscopy (EIS) measurements. The CV curves were performed at different scan rates varying from 10 to 100 mV s<sup>-1</sup> at potentials between 0 and 1.0 V with a LK98B II microcomputer-based electro-chemical analyzer (LANLIKE). The galvanostatic charge/discharge was carried out with a supercapacitor tester (Arbin MSTAT, USA). Impedance spectroscopies were measured in the range of from 100 kHz to 10 mHz using Autolab (Metrohm). All the electrochemical tests were carried out at room temperature.

The gravimetric specific capacitance,  $C_{sp}$  (F g<sup>-1</sup>), was calculated from galvanostatic charge/discharge test according to the formula  $C_{sp} = \frac{2I}{m dV/dt}$ , where  $I$  is the constant current,  $m$  is the mass of carbon in each electrode, and  $dV/dt$  is calculated from the slope obtained by fitting a straight line to the discharge curve over the range of  $V$  (the voltage at the beginning of discharge) to  $\frac{1}{2} V$ .

The electronic conductivities of NG and RG were tested in an indirect way as following method. Typically, the material was mixed with 4 wt.% PTFE as a binder, and homogenized in an agate mortar. Then it was rolled into 10–20  $\mu$ m thickness sheets and cut into 3 $\times$ 1 cm<sup>2</sup> and pressed at 10 MPa for 10 s. Then it was covered with the copper foil on both sides and tested using a multimeter. The electronic conductivity of the film was calculated using the formula  $\lambda = L/R_x \cdot W \cdot d$ , where  $\lambda$  is the electronic conductivity of sample,  $L$ ,  $W$ ,  $d$  is the length, width and thickness of the sheet and  $R_x$  is the resistance of the sheet tested by the multimeter.

## 3. Results and discussion

### 3.1. Morphology and structure characterization

Optical photographs and the SEM images of the materials are shown in Fig. 2. Fig. 2a indicates that the typical product is in a form of strong self-assembled hydrogel column with a diameter about 2 cm and a height of 4 cm. The hydrogel column is two times volume of that formed from normal OPD-free GO suspension under the same condition (inset of Fig. 2a), which can be explained that the existence of OPD will effectively prevent the self-stacked behavior of GO during the hydrothermal process, and accordingly help to form large volume of three-dimensional (3D) graphene [38]. The SEM images of RG and NG are shown in Fig. 2b and c, respectively. Compared with RG, NG exhibits interconnected 3D porous structure, indicating the effectiveness of OPD for the prevention of restacking of graphene sheets. Nevertheless, the RG are partly aggregated due to the  $\pi$ - $\pi$  stacking among individual graphene sheets. In order to study the distribution of nitrogen in NG, the elemental mapping was performed. The nitrogen mapping image (Fig. 2f), in accordance with carbon's (Fig. 2e), actually reflects the morphology of the selective area in Fig. 2d. The result confirms that the nitrogen atoms are uniformly distributed in the framework of graphene.

Fig. 3 shows the TEM images of GO, RG and NG. It can be clearly seen that the GO exhibits a typical exfoliated nanostructure with a rather flat and smooth flake-like morphology with several layers stacked. Compared with GO, the RG and NG sheets are randomly aggregated, thin and crumpled, interconnected with each other, resembling rippled silk waves [41], which could be attributed to the hydrothermal process [45].

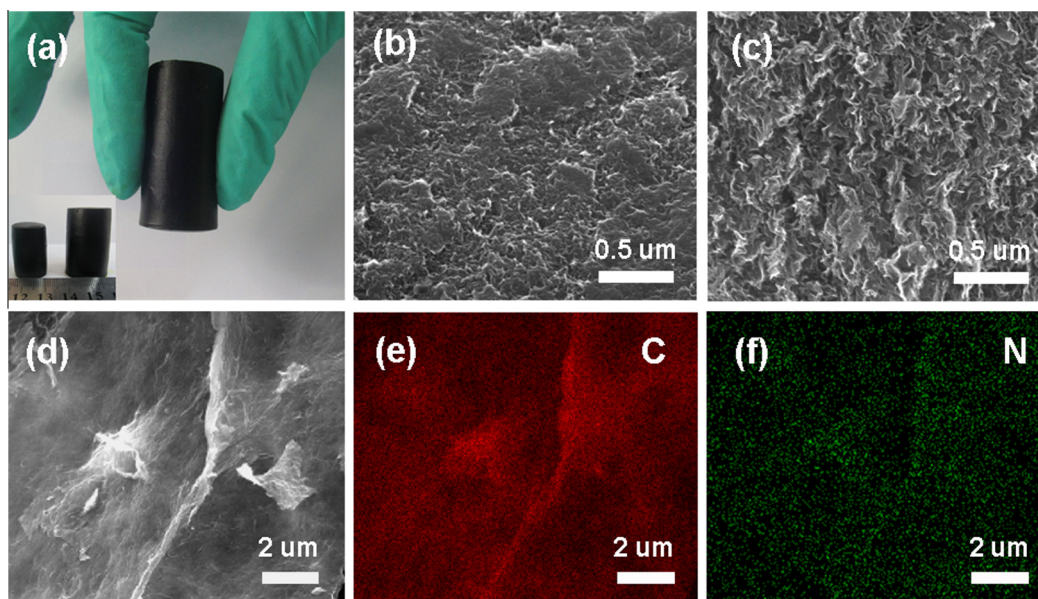


**Fig. 2 – (a) Optical photograph of the hydrogel column of NG, inset is the comparison graphs of RG (left) and NG (right); (b) SEM image of RG; (c, d) SEM images of NG; (e, f) Carbon and nitrogen mapping images of NG for (d).**

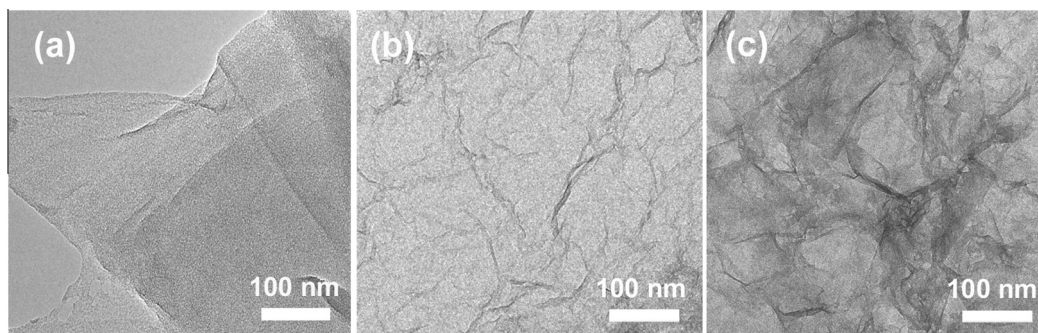


**Fig. 3 – TEM images of (a) GO; (b) RG; (c) NG.**

Furthermore, the ripples of NG are slightly deeper than RG's, which may originate from the heteroatoms or defects remained in the plane of grapheme [45,46]. These relatively deeper crumpled structures of NG may easily form a 3D conducting network for fast electron transfer between the active electrode materials and the current collector [41] and thus would contribute to improve the electrochemical performance.

Raman spectra offer clear evidence of N-doping in the graphene lattice. As shown in Fig. 4a, the G peaks of RG and NG appear at 1597 and 1591  $\text{cm}^{-1}$ , respectively. The downshift of the G peak from RG to NG, and the  $I_D/I_G$  ratio increase from 0.86 for RG to 0.99 for NG both indicate that nitrogen atoms have been doped into graphene, which are consistent with previous reports in the literatures [34,47]. In addition, the peak at 1518  $\text{cm}^{-1}$  emerging as a shoulder of G band at a lower frequency is considered to be the Raman feature induced from phenazine structure in NG [48]. The chemical structure of NG was further investigated by FT-IR spectroscopy. As shown in Fig. 4b, the carbonyl stretching mode of carboxyl groups at 1724  $\text{cm}^{-1}$  and the breathing vibration mode of

the epoxy groups at 1201  $\text{cm}^{-1}$  are observed in RG [40]. However, in the spectrum of NG, the peaks at 1724 and 1201  $\text{cm}^{-1}$  disappear, which may be explained that in the presence of OPD, the oxygen containing functional groups in GO would react with the  $-\text{NH}_2$  in OPD to generate other covalent bonds. Furthermore, the new peaks at 1636, 1566, 1194 and 747  $\text{cm}^{-1}$  appear. The peaks at 1636 and 1566  $\text{cm}^{-1}$  are attributed to the skeletal stretching vibration mode of quinoid and benzoid rings in phenazine [49]. The peak at 1194  $\text{cm}^{-1}$  and the other one at 747  $\text{cm}^{-1}$  in the fingerprint spectrum region also can be assigned to the characteristic peaks of phenazine [48]. For comparison, the IR spectrum of the simple adsorption products of RG hydrogel and OPD (RG/OPD) was provided. The difference between NG and RG/OPD is very obvious. Firstly the carboxyl group peak does not disappear but shifts down to 1707 from 1724  $\text{cm}^{-1}$ , which shows that the hydrogen bond, not the covalent bond, was formed between  $-\text{COOH}$  and  $-\text{NH}_2$ . Then the epoxy groups' peak at about 1200  $\text{cm}^{-1}$  show hardly any change. Furthermore, the skeletal stretching vibration mode of quinoid rings of phenazine doesn't exist in GO/OPD. It is worth to note that

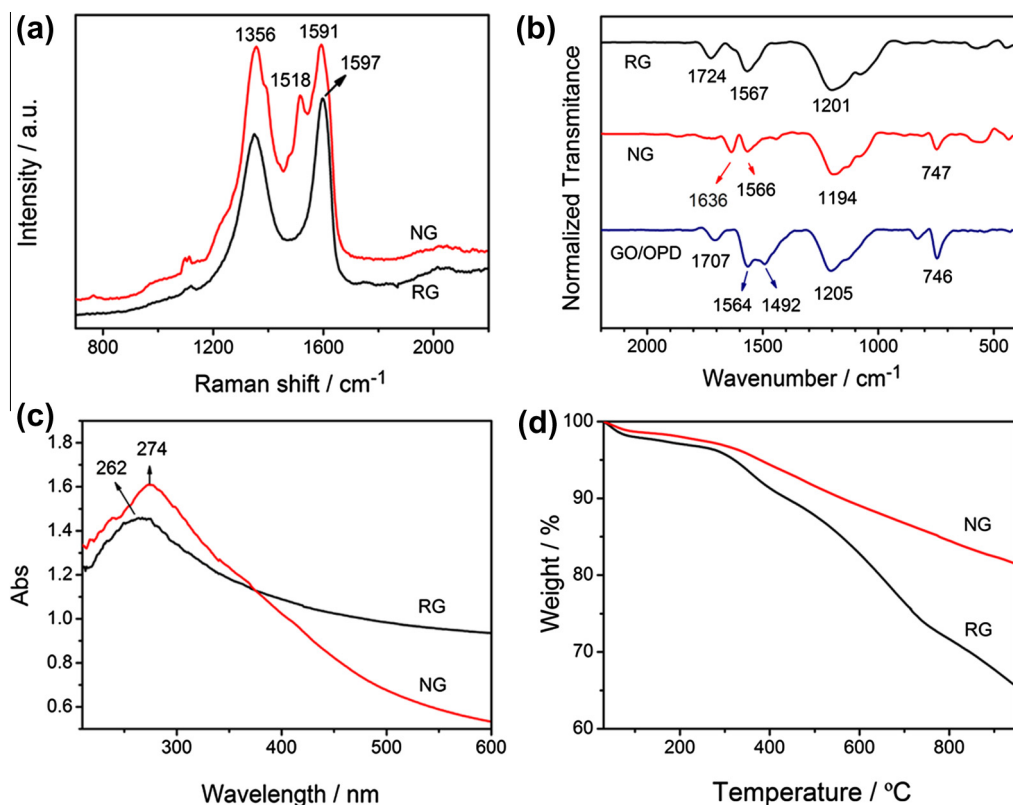


Fig. 4 – (a) Raman, (b) IR, (c) UV-vis spectra and (d) TGA of NG and RG.

the peaks at 1492 and 746  $\text{cm}^{-1}$  are attributed to the skeletal vibration mode of benzene rings and the bending vibration mode of C–H in 1,2-substituted benzene rings, respectively. The IR characterizations demonstrate that the phenazine structure in NG has been actually formed in the hydrothermal process. The UV-vis spectra are shown in Fig. 4c, where the absorption peaks of RG and NG appear at 265 and 274 nm, respectively. The red-shift of the peak from RG to NG can be attributed to the electron-donating capability of nitrogen heteroatom. All of the spectrum characteristics of Raman, FT-IR and UV-vis confirm that the nitrogen containing covalent bonds between graphene and OPD are formed in the solvothermal process and there exist the phenazine structures. The thermostabilities of NG and RG were also studied by TGA. As shown in Fig. 4d, RG shows 35 wt.% mass loss at the temperature of up to 950 °C due to the decomposition of the oxygen containing groups, which partially remained in the solvothermal process. However, compared to RG, NG shows only 19 wt.% weight loss, which is significantly smaller than RG. The TGA results indicate a higher thermal stability of NG than RG, which could be attributed to the formation of plenty of nitrogen containing functional groups in NG, especially the phenazine structures, which are more stable than the oxygen containing ones in RG.

The content of nitrogen in NG was determined by elemental analysis and it reaches 7.7 atom%. The elemental composition of NG was further characterized using XPS measurements, shown in Fig. 5. The spectrum of NG (Fig. 5a) shows a nitrogen component (399 eV) in addition to the carbon (284 eV) and oxygen species (532 eV), while only

carbon and oxygen species were detected for GO. The high resolution C1s spectra of original GO (Fig. 5b) consists of three peaks arising from C–C (284.6 eV), C–O (286.7 eV) and O–C=O (288.4 eV). After the solvothermal reaction, an additional type of carbon at about 285.6 eV is observed (Fig. 5c), which originates from C–N [41]. According to the high resolution N1s spectra of NG (Fig. 5d), mainly two kinds of nitrogen were doped. The peak at 398.8 eV is attributed to the –N= bond in phenazine [50] and the peak at 399.8 eV can be ascribed to the –NH– bond in benzimidazole groups [51]. This also confirms that the types of nitrogen in NG are phenazine-N and benzimidazole-N. Accompany with the appearance of phenazine-N, the structure of the double-N atoms in the same hexagon of the graphene skeleton is formed and this is the meaning of double-N doped. One of the functions of phenazine-N is that it could enhance the electronic conductivity of graphene in comparison with the non doped ones. This can be confirmed by the measurements of intrinsic electronic conductivity of NG and RG, which shows 5.46  $\text{S m}^{-1}$  for NG and 0.48  $\text{S m}^{-1}$  for RG. The inherent higher electronic conductivity of NG could also make contribution for a good electrochemical performance for its supercapacitors.

### 3.2. Electrochemical performance characterization

Two-electrode test cell configuration was used as an accurate and recommended method to measure the obtained materials' supercapacitor performance. The performances of NG- and RG-based supercapacitor (named NGSC and RGSC, respectively) were analyzed using CV, galvanostatic charge/

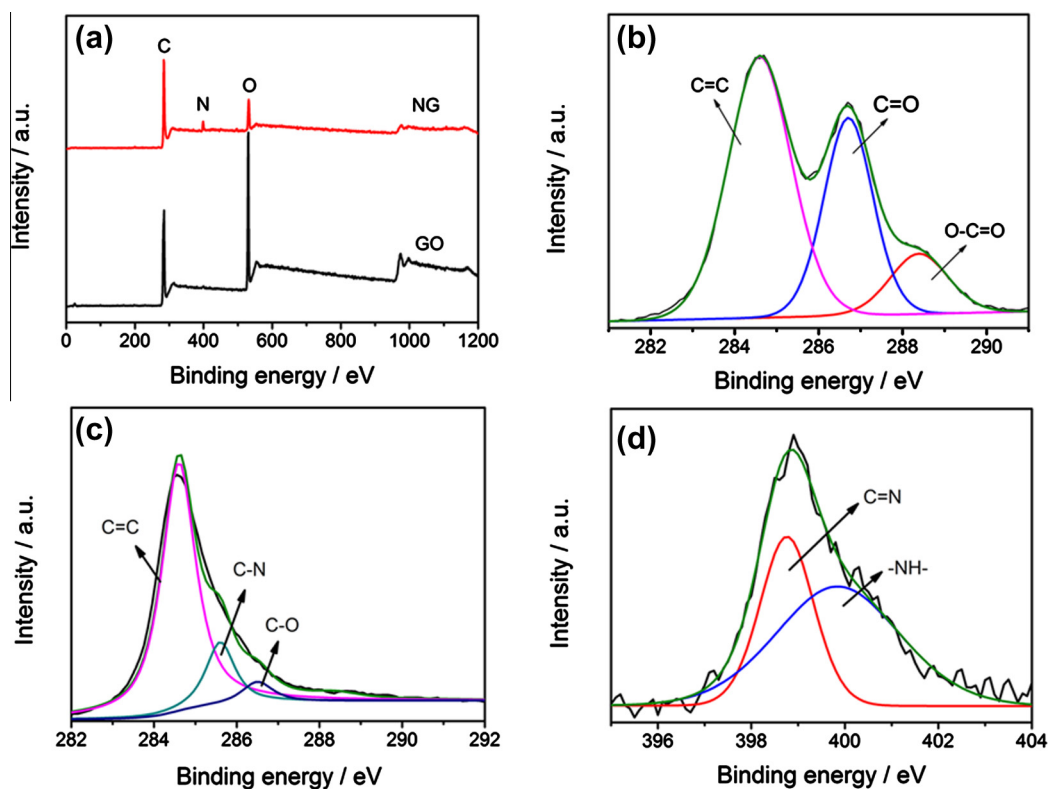


Fig. 5 – XPS spectra of (a) Survey spectra of GO and NG; (b) High resolution C1s spectra of GO and (c) NG; (d) N1s spectra of NG.

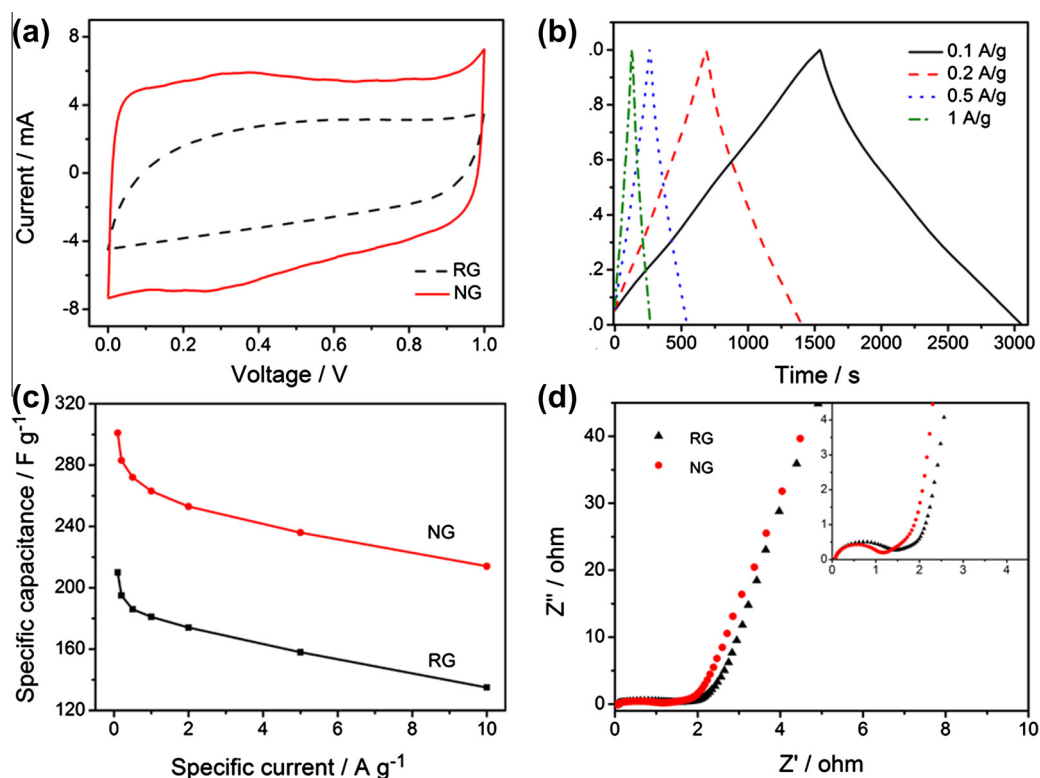
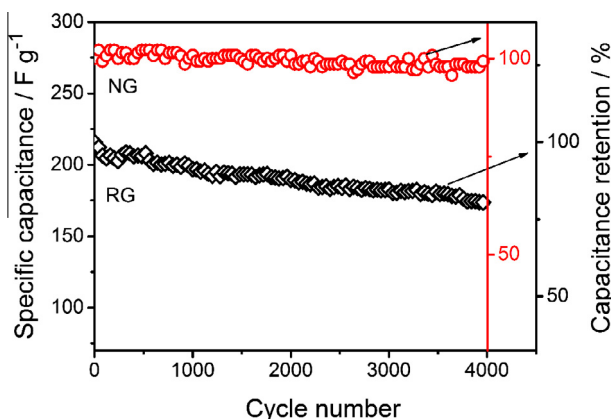


Fig. 6 – Electrochemical performance of the supercapacitors: (a) CV curves of RGSC and NGSC measured at the scan rate of  $10 \text{ mV s}^{-1}$  in the potential range of 0.0–1.0 V; (b) Galvanostatic charge/discharge curves for NGSC tested at different current densities from 0.1 to  $1 \text{ A g}^{-1}$ ; (c) Rate performances of NGSC and RGSC; (d) Nyquist plots of NGSC and RGSC, and the inset shows the expanded high-frequency region of the plots.



**Fig. 7 – The comparison of cycling stabilities for NGSC and RGSC charge–discharged after 4000 cycles, measured at a current density of  $1 \text{ A g}^{-1}$  within the potential range from 0 to 1.0 V.**

discharge and EIS. Fig. 6a presents the CV curves of RGSC and NGSC in 6 M KOH aqueous electrolyte at the scan rate of  $10 \text{ mV s}^{-1}$  and near rectangular voltammetry characteristics could be observed. Obviously, NGSC exhibits a much higher capacitive response than RGSC, indicating that nitrogen doping enhances the electrochemical activity of grapheme materials. Notably, the CV curve of NGSC shows the Faradic redox peaks, which are at  $\sim 0.35 \text{ V}$  of anodic scan and  $\sim 0.25 \text{ V}$  of cathodic scan respectively, corresponding to the redox reactions of electrochemically active functional groups on the surface of electrode. These results demonstrate that the capacitive response of NGSC is from the combination of EDLC and pseudo-capacitance [37]. The specific capacitance ( $C_{sp}$ ) of the electrode materials were calculated from galvanostatic discharge curves (Fig. 6b). The  $C_{sp}$  value for NG is  $301 \text{ F g}^{-1}$  at a current density of  $0.1 \text{ A g}^{-1}$ , which is significantly larger than that of the compared RG materials ( $210 \text{ F g}^{-1}$  at  $0.1 \text{ A g}^{-1}$ ) and also much higher than that of other reported NG materials [40,47]. The capacitive response of NG would be from the combination of redox reactions of benzimidazole and the electrochemical double-layer capacitance. Furthermore, the  $C_{sp}$  value of NG still remains as high as  $214 \text{ F g}^{-1}$  even at a high current density of  $10 \text{ A g}^{-1}$ , indicating an excellent rate capability of the NGSC. The charge/transfer resistance and ion diffusion performance were obtained by EIS measurements at a frequency range of 100 kHz–10 mHz. Fig. 6d shows the Nyquist plots for NGSC and RGSC. In the low-frequency region, both NGSC and RGSC plots present an oblique line, suggesting that the electrode process is under diffusion control. And the slope of the plot for NGSC is steeper than RGSC's, indicating that the formation rate of the electric double layers of NGSC is higher and it is easier to form the ideal EDLC than RGSC [52]. The slope of the  $45^\circ$  portion of the curve in the high frequency range called the Warburg resistance implies the frequency dependence of ion diffusion in the electrolyte. The Warburg curve of NGSC is shorter than RGSC's, indicating the shorter ion diffusion path for NGSC [7]. In the high-frequency region, NGSC exhibits a smaller semi-circle than RGSC and the equivalent series resistance of NGSC is extremely small ( $0.068 \Omega$ ), indicating the lower charge-

**Table 1 – Carbon, hydrogen, nitrogen and oxygen contents (wt.%) in RG and NG from elementary analysis.**

Sample	C (wt.%)	H (wt.%)	N (wt.%)	O (wt.%)
RG	73.6	1.7	0	24.7
NG	80.4	2.0	7.2	10.4

transfer resistance and an excellent electronic conductivity [37]. In short, the desirable excellent supercapacitor performance of NGSC can be attributed to the high nitrogen level and suitable nitrogen types, which can offer pseudo-capacitance and excellent electronic conductivity.

The cycling stabilities of NGSC and RGSC were also evaluated using the galvanostatic charge/discharge technique at a current density of  $1 \text{ A g}^{-1}$  (Fig. 7). The NGSC maintains around 97.1% (coulombic efficiency  $\eta = 99.2\%$ ) of their corresponding initial specific capacity after 4000 cycles. In contrast, RGSC retains only about 79.6% ( $\eta = 99.0\%$ ). The difference of stabilities of NGSC and RGSC could be caused by different internal structure of the two kinds of active electrode materials. In order to further illustrate the superior cycling stability of NG, the elemental analysis of RG and NG has been performed, and the percentage mass contents of the elements are shown in Table 1. In RG, the O content reaches up to 24.7%, which means that the large amount of oxygen containing functional groups would cause irreversible redox reactions during the electrochemical cycling process and thus reduce the cycling stability. Correspondingly, in NG, the O content has decreased to be only 10.4% and the oxygen containing functional groups is reduced, as most of them were replaced in the doping process by the nitrogen ones, such as benzimidazole-N and phenazine-N. Therefore, with the reversible reactions of benzimidazole-N [25] and excellent electronic conductivity of phenazine-N, our NG materials have a much improved electrochemical stability and a higher degree of reversibility.

#### 4. Conclusion

We have demonstrated an efficient route to prepare NG materials through a one-step solvothermal reaction using OPD as the double-N dopant. The benzimidazole-N and phenazine-N structures formed in the doping process. Because of their high nitrogen level, appropriate nitrogen species and excellent electronic conductivity, the NG materials display a high specific capacitance up to  $301 \text{ F g}^{-1}$  in addition to maintaining excellent rate capability and cycling stability. Therefore, our NG materials could be applied for high-performance supercapacitors.

#### Acknowledgements

The authors gratefully acknowledge financial support from MOST (Grants 2012CB933401 and 2011DFB50300), NSFC (Grants 50933003 and 51273093), Science and Technology Research Project of Higher Education of Hebei Province (Grant z2012064), Science Research Project of Langfang Teachers College (Grant LSZQ200908).

## REFERENCES

- [1] Zhang L, Yang X, Zhang F, Long G, Zhang T, Leng K, et al. Controlling the effective surface area and pore size distribution of  $sp^2$  carbon materials and their impact on the capacitance performance of these materials. *J Am Chem Soc* 2013;135(15):5921–9.
- [2] Zhang F, Zhang T, Yang X, Zhang L, Leng K, Huang Y, et al. A high-performance supercapacitor-battery hybrid energy storage device based on graphene-enhanced electrode materials with ultrahigh energy density. *Energy Environ Sci* 2013;6:1623–32.
- [3] Zhang L, Zhang F, Yang X, Leng K, Huang Y, Chen Y. High-performance supercapacitor electrode materials prepared from various pollens. *Small* 2013;9(8):1342–7.
- [4] Zhang L, Zhao X. Carbon-based materials as supercapacitor electrodes. *Chem Soc Rev* 2009;38:2520–31.
- [5] Huang Y, Liang J, Chen Y. An overview of the applications of graphene-based materials in supercapacitors. *Small* 2012;8(12):1805–34.
- [6] Stoller MD, Park S, Zhu Y, An J, Ruoff RS. Graphene-based ultracapacitors. *Nano Lett* 2008;8(10):3498–502.
- [7] Wang Y, Shi Z, Huang Y, Ma Y, Wang C, Chen M, et al. Supercapacitor devices based on graphene materials. *J Phys Chem C* 2009;113:13103–7.
- [8] Lv W, Tang D, He Yg, You C, Shi Z, Chen X, et al. Low-temperature exfoliated graphenes: vacuum-promoted exfoliation and electrochemical energy storage. *ACS Nano* 2009;3(11):3730–6.
- [9] Lin Z, Liu Y, Yao Y, Hildreth OJ, Li Z, Moon K, et al. Superior capacitance of functionalized graphene. *J Phys Chem C* 2011;115:7120–5.
- [10] Zhu Y, Stoller MD, Cai W, Velamakanni A, Piner RD, Chen D, et al. Exfoliation of graphite oxide in propylene carbonate and thermal reduction of the resulting graphene oxide platelets. *ACS Nano* 2010;4(2):1227–33.
- [11] Liu C, Yu Z, Neff D, Zhamu A, Jang BZ. Graphene-based supercapacitor with an ultrahigh energy density. *Nano Lett* 2010;10:4863–8.
- [12] Miller JR, Outlaw RA, Holloway BC. Graphene double-layer capacitor with ac line-filtering performance. *Science* 2010;329:1637–9.
- [13] Yang X, Zhang F, Zhang L, Zhang T, Huang Y, Chen Y. A high-performance graphene oxide-doped ion gel as gel polymer electrolyte for all-solid-state supercapacitor application. *Adv Funct Mater* 2013;23(26):3353–60.
- [14] Zhang L, Zhang F, Yang X, Long G, Wu Y, Zhang T, et al. Porous 3D graphene-based bulk materials with exceptional high surface area and excellent conductivity for supercapacitors. *Sci Rep* 2013;3:1408–16.
- [15] Deng W, Ji X, Chen Q, Banks CE. Electrochemical capacitors utilising transition metal oxides: an update of recent developments. *RSC Adv* 2011;1:1171–8.
- [16] Zhang G, Wang D, Li F, Zhang L, Li N, Wu Z, et al. Graphene-wrapped  $Fe_3O_4$  anode material with improved reversible capacity and cyclic stability for lithium ion batteries. *Chem Mater* 2010;22:5306–13.
- [17] Yan J, Fan Z, Wei T, Qian W, Zhang M, Wei F. Fast and reversible surface redox reaction of graphene- $MnO_2$  composites as supercapacitor electrodes. *Carbon* 2010;48(13):3825–33.
- [18] Wu Z, Wang D, Ren W, Zhao J, Zhou G, Li F, et al. Anchoring hydrous  $RuO_2$  on graphene sheets for high-performance electrochemical capacitors. *Adv Funct Mater* 2010;20:3595–602.
- [19] Lai L, Yang H, Wang L, Teh BK, Zhong J, Chou H, et al. Preparation of supercapacitor electrodes through selection of graphene surface functionalities. *ACS Nano* 2012;6(7):5941–51.
- [20] Gómez H, Ram MK, Alvi F, Villalba P, Stefanakos E, Kumara A. Graphene-conducting polymer nanocomposite as novel electrode for supercapacitors. *J Power Sources* 2011;196(8):4102–8.
- [21] Zhang L, Xiong Z, Zhao X. A composite electrode consisting of nickel hydroxide, carbon nanotubes, and reduced graphene oxide with an ultrahigh electrocapacitance. *J Power Sources* 2013;222:326–32.
- [22] Wu Y, Zhang T, Zhang F, Wang Y, Ma Y, Huang Y, et al. In situ synthesis of graphene/single-walled carbon nanotube hybrid material by arc-discharge and its application in supercapacitors. *Nano Energy* 2012;1:820–7.
- [23] Wang Y, Wu Y, Huang Y, Zhang F, Yang X, Ma Y, et al. Preventing graphene sheets from restacking for high-capacitance performance. *J Phys Chem C* 2011;115:23192–7.
- [24] Wu Z, Winter A, Chen L, Sun Y, Turchanin A, Feng X, et al. Three-dimensional nitrogen and boron co-doped graphene for high-performance all-solid-state supercapacitors. *Adv Mater* 2012;24:5130–5.
- [25] Guo H, Su P, Kang X, Ning S. Synthesis and characterization of nitrogen-doped graphene hydrogels by hydrothermal route with urea as reducing-doping agents. *J Mater Chem A* 2013;1:2248–55.
- [26] Wu Z, Ren W, Xu L, Li F, Cheng H. Doped graphene sheets as anode materials with superhigh rate and large capacity for lithium ion batteries. *ACS Nano* 2011;5(7):5463–71.
- [27] Hassan FM, Chabot V, Li J, Kim BK, Ricardez-Sandoval L, Yu A. Pyrrolic-structure enriched nitrogen doped graphene for highly efficient next generation supercapacitors. *J Mater Chem A* 2013;1:290–2912.
- [28] Palaniselvam T, Aiyappa HB, Kurungot S. An efficient oxygen reduction electrocatalyst from graphene by simultaneously generating pores and nitrogen doped active sites. *J Mater Chem* 2012;22:23799–805.
- [29] Jeong HM, Lee JW, Shin WH, Choi YJ, Shin HJ, Kang JK, et al. Nitrogen-doped graphene for high-performance ultracapacitors and the importance of nitrogen-doped sites at basal planes. *Nano Lett* 2011;11:2472–7.
- [30] Xue Y, Wu B, Jiang L, Guo Y, Huang L, Chen J, et al. Low temperature growth of highly nitrogen-doped single crystal graphene arrays by chemical vapor deposition. *J Am Chem Soc* 2012;134:11060–3.
- [31] Panchakarla LS, Subrahmanyam KS, Saha SK, Govindaraj A, Krishnamurthy HR, Waghmare UV, et al. Synthesis, structure, and properties of boron- and nitrogen-doped graphene. *Adv Mater* 2009;21:4726–30.
- [32] Wang C, Zhou Y, He L, Ng TW, Hong G, Wu Q, et al. In situ nitrogen-doped graphene grown from polydimethylsiloxane by plasma enhanced chemical vapor deposition. *Nanoscale* 2013;5:600–5.
- [33] Wang X, Li X, Zhang L, Yoon Y, Weber PK, Wang H, et al. N-doping of graphene through electrothermal reactions with ammonia. *Science* 2009;324:768–71.
- [34] Lin Z, Waller G, Liu Y, Liu M, Wong CP. Facile synthesis of nitrogen-doped graphene via pyrolysis of graphene oxide and urea, and its electrocatalytic activity toward the oxygen-reduction reaction. *Adv Energy Mater* 2012;2:884–8.
- [35] Sheng Z, Shao L, Chen J, Bao W, Wang F, Xia X. Catalyst-free synthesis of nitrogen-doped graphene via thermal annealing graphite oxide with melamine and its excellent electrocatalysis. *ACS Nano* 2011;5(6):4350–8.
- [36] Wen Z, Wang X, Mao S, Bo Z, Kim H, Cuiet S, et al. Crumpled nitrogen-doped graphene nanosheets with ultrahigh pore volume for high-performance supercapacitor. *Adv Mater* 2012;24:5610–6.

- [37] Sun L, Wang L, Tian C, Tan T, Xie Y, Shi K, et al. Nitrogen-doped graphene with high nitrogen level via a one-step hydrothermal reaction of graphene oxide with urea for superior capacitive energy storage. *RSC Adv* 2012;2:4498–506.
- [38] Zhao Y, Hu C, Hu Y, Cheng H, Shi G, Qu L. A versatile, ultralight, nitrogen-doped graphene framework. *Angew Chem* 2012;51(45):11371–5.
- [39] Chen P, Yang J, Li S, Wang Z, Xiao T, Qian Y. Hydrothermal synthesis of macroscopic nitrogen-doped graphene hydrogels for ultrafast supercapacitor. *Nano Energy* 2013;2(2):249–56.
- [40] Lee JW, Kob JM, Kima JD. Hydrothermal preparation of nitrogen-doped graphene sheets via hexamethylenetetramine for application as supercapacitor electrodes. *Electrochim Acta* 2012;85:459–66.
- [41] Ai W, Zhou W, Du Z, Du Y, Zhang H, Jia X, et al. Benzoxazole and benzimidazole heterocycle-grafted graphene for high-performance supercapacitor electrodes. *J Mater Chem* 2012;22:23439–46.
- [42] Zhang L, Liang J, Huang Y, Ma Y, Wang Y, Chen Y. Size-controlled synthesis of graphene oxide sheets on a large scale using chemical exfoliation. *Carbon* 2009;47:3365–8.
- [43] Stoller MD, Ruoff RS. Best practice methods for determining an electrode material's performance for ultracapacitors. *Energy Environ Sci* 2010;3:1294–301.
- [44] Gogotsi Y, Simon P. True performance metrics in electrochemical energy storage. *Science* 2011;334:917–8.
- [45] Long D, Li W, Ling L, Miyawaki J, Mochida I, Yoon SH. Preparation of Nitrogen-doped graphene sheets by a combined chemical and hydrothermal reduction of graphene oxide. *Langmuir* 2010;26:16096–102.
- [46] Lee YH, Chang KH, Hu GC. Differentiate the pseudocapacitance and double-layer capacitance contributions for nitrogen-doped reduced graphene oxide in acidic and alkaline electrolytes. *J Power Sources* 2013;227:300–8.
- [47] Yan J, Xiao Y, Ning G, Wei T, Fan Z. Facile and rapid synthesis of highly crumpled graphene sheets as high-performance electrodes for supercapacitors. *RSC Adv* 2013;3:2566–71.
- [48] Sestrem RH, Ferreira DC, Landers R, Temperini MLA, Nascimento GM. Synthesis and spectroscopic characterization of polymer and oligomers of ortho-phenylenediamine. *Eur Polym J* 2010;6:484–93.
- [49] Wang Z, Liao F, Yang S, Guo T. A novel route synthesis of poly(ortho-phenylenediamine) fluffy microspheres self-assembled from nanospheres. *Fiber Polym* 2011;12(8):997–1001.
- [50] Lositoa I, Malitestab C, Baric ID, Calvano CD. X-ray photoelectron spectroscopy characterization of poly(2,3-diaminophenazine) films electrosynthesised on platinum. *Thin Solid Films* 2005;473:104–13.
- [51] Unni SM, Devulapally S, Karjulea N, Kurungot S. Graphene enriched with pyrrolic coordination of the doped nitrogen as an efficient metal-free electrocatalyst for oxygen reduction. *J Mater Chem* 2012;22(44):23506–13.
- [52] Qiu Y, Zhang X, Yang S. High performance supercapacitors based on highly conductive nitrogen-doped graphene sheets. *Phys Chem Chem Phys* 2011;13:12554–8.